Phys. Status Solidi B **251,** No. 10, 2027–2033 (2014) / **DOI** 10.1002/pssb.201350360

Part of Special Issue on
Ferroic Glasses: Magnetic, Polar and Strain Glass

physica status solidi b
www.pss-b.com
basic solid state physics

High temperature strain glass transition in defect doped Ti–Pd martensitic alloys

Yumei Zhou[1], Dezhen Xue*[,1], Xiangdong Ding[1], Kazuhiro Otsuka[2], Jun Sun[1], and Xiaobing Ren[1,2]

[1] Multi-disciplinary Materials Research Center, Frontier Institute of Science and Technology, State Key Laboratory for Mechanical Behavior of Materials, Xi'an Jiaotong University, Xi'an 710049, P. R. China
[2] Ferroic Physics Group, National Institute for Materials Science, Tsukuba 305-0047 Ibaraki, Japan

Received 27 November 2013, revised 28 March 2014, accepted 28 March 2014
Published online 2 May 2014

Keywords damping, glass transitions, martensitic transformations, point defects, strain glasses

* Corresponding author: e-mail xuedezhen@mail.xjtu.edu.cn, Phone: +86 2982668610, Fax: +86 2982663453

Strain glass alloys exhibit novel functionalities around their glass transition temperature T_0; but T_0 is too low for TiNi-based strain glass alloys, restricting their potential applications. It is thus of practical importance to develop high T_0 strain glass alloys. In the present study, several ambient-temperature T_0 strain glass alloys were developed, by selecting TiPd with high temperature martensitic transformation as the host alloy and doping different kinds of point defects to substitute Pd. By comparing TiPd-based and TiNi-based strain glass alloys, it is found that T_0 of strain glass alloys is controlled by the martensitic transformation temperature of its host alloys without defect doping. Finally, our results suggest that strain glass alloys are also promising damping materials for applications, as their transition damping peak is insensitive to the cooling/heating rate and is also thermal hysteresis free.

1 Introduction Strain glass (STG), a glassy state in ferroelastic/martensitic systems, was initially observed in Ni-rich $Ti_{50-x}Ni_{50+x}$ alloys where the high temperature B2 structure appeared to persist to 0 K above a critical defect concentration $x = 1.5$ at% [1]. The randomness produced by the defects frustrates the system so that the long-range strain ordering becomes inaccessible [1–6]. Such a glassy state is analogous to the well-known frozen disordered state in other ferroic systems such as cluster spin glass in ferromagnetic system or ferroelectric relaxor in ferroelectric system [7–9]. These glassy states in ferroic materials are generally termed as "ferroic glass" [10].

The glassy features of strain glass are manifested in its mechanical response [11–14]. For instance, the frequency dependence of the AC properties (the storage modulus and internal friction) was probed by the dynamic mechanical analysis (DMA) experiments [12], and the breaking down of ergodicity was measured by zero-field-cooling/field-cooling (ZFC/FC) experiments on DC properties (strain) [11]. Recent high resolution transmission electron microscopy (HREM) results further reveal that a nano-scale local displacive transition takes place around the glass transition temperature in strain glass alloys [15, 16]. In addition, several numerical simulations and theoretical models have been proposed for the formation of strain glass in the presence of disorder [3, 5, 17–21].

Besides these investigations on the nature of strain glass, such "glassy" martensite exhibits several unique functionalities such as the unexpected shape memory effect (SME), and superelasticity (SE) of the "non-martensitic" system [12, 22], and the stress tuned intelligent damping properties [23]. These functionalities depend sensitively on the glass transition temperature, around which the stress-induced strain glass to long-range-strain-ordered martensitic transformation could take place [2, 23]. Up to now, the strain glass has been identified in numerous alloys by means of compositional variations (doping point defects) or aging induced nano-sized precipitates [13, 24]. Nevertheless, most of the reported strain glass alloys possess fairly low glass transition temperature, for instance, about 160 K for TiNi-based systems [4, 13, 25], which limits their potential applications [26]. Thus, it is of interest to search for strain glass with high glass transition temperature.

Recent studies on $Ti_{50}(Pd_{50-x}Cr_x)$ shape memory alloy and $Ni_{55-x}Co_xMn_{20}Ga_{25}$ Heusler alloy showed that the glass transition in these alloys can take place around room temperature [12, 14]. Especially, for the $Ti_{50}(Pd_{40}Cr_{10})$ strain glass alloy, the undoped host TiPd alloy undergoes a

B2–B19 martensitic transformation with very high martensitic transformation temperature (M_s) of 810 K. Such situation indicates a positive relation between the M_s of the host alloy and the glass transition temperature of the doped alloy [12].

In the present study, we further confirmed the occurrence of strain glass transition in defect doped TiPd systems, despite of different kinds of point defects (Fe, Mn). The corresponding glass transition temperature in these strain glass alloys is shifted to ambient temperature range. We then discuss the possible relationship of the glass transition temperature with the M_s, size of twin shear and elastic anisotropy factor of its host alloy. The present work is likely to suggest a guideline for designing new strain glass alloys with required strain glass transition temperature. Furthermore, our results suggest that strain glass alloys are also promising damping materials as their transition damping peak is insensitive to thermal gradient and is also thermal hysteresis free.

2 Experimental procedures A series of $Ti_{50}(Pd_{50-x}D_x)$ alloys with defect concentration $x = 5$–16 at% were tested in our study. D (Fe, Mn,) is designed to substitute for Pd and acts as point defect. Base ingots were made by induction melting a mixture of 99.9% pure Ti, 99.9% pure Pd, and 99.9% pure D in an argon atmosphere. Specimens for measurement were spark cut from the ingots. Then they were solution-treated at 1373 K for 1 h in evacuated quartz tubes, followed by water quenching. All the specimens were mechanically polished and chemically etched, in order to remove the affected surface layer.

Differential scanning calorimetry (DSC) measurements were made with a cooling/heating rate of 10 K min^{-1} to detect the martensitic transition with exothermal/endothermic peaks as well as the transition latent heat change associated with the martensitic transition. Multi-frequency DMA was carried out to test the strain glass transition in a single cantilever mode with constant displacement amplitude of 15 μm. The values of internal friction and storage modulus were recorded for six frequencies (0.2, 0.4, 1, 4, 10, and 20 Hz) as a function of temperature, with a cooling and heating rate of 2 K min^{-1}.

3 Experimental results

3.1 Evolution of transformation behaviors of $Ti_{50}(Pd_{50-x}D_x)$ alloys with increasing defect concentration As mentioned in the introduction part, the formation of strain glass is due to the existence of point defects, which suppresses the formation of long-range-strain-ordered martensite phase [2]. We first explored the effect of defect doping on the martensitic transformation behavior of these $Ti_{50}(Pd_{50-x}Fe_x)$ and $Ti_{50}(Pd_{50-x}Mn_x)$ alloys by comparing the DSC results.

As shown in Fig. 1a and b, the exothermal/endothermic peaks in DSC results and large hysteresis associated with the transformation (>18 K) suggest that both $Ti_{50}(Pd_{42}Fe_8)$ and $Ti_{50}(Pd_{38}Fe_{12})$ undergo a B2–B19 martensitic transformation. It is shown that with increasing Fe concentration, the onset temperature of normal martensitic transformation (M_s), indicating the martensitic stability was reduced greatly by the Fe doping. The corresponding transformation latent heat obtained from both cooling and heating processes decreases as well when Fe concentration increases. For alloys with Fe concentration more than ~14 at% (as shown in Fig. 1c and d), DSC peak virtually vanishes, suggesting the absence of normal martensitic transformation.

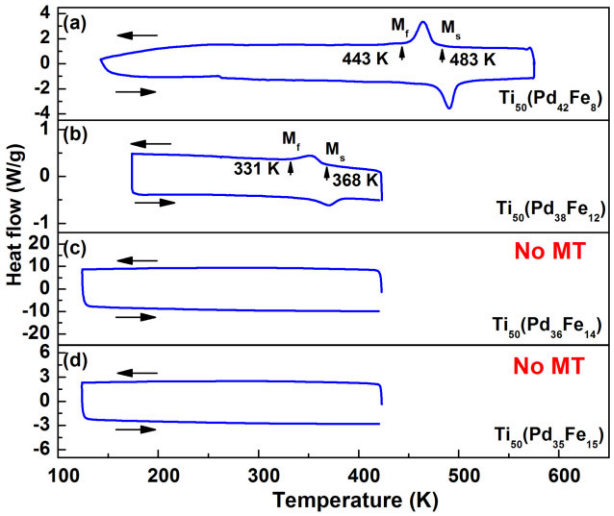

Figure 1 (a–d) DSC curves of $Ti_{50}(Pd_{50-x}Fe_x)$ ($x = 8$, 12, 14, 15) alloys, respectively. MT represents the martensitic transformation. M_s and M_f stand for the starting and finishing temperature of B2–B19 martensitic transformation, respectively.

The similar evolution of transformation behavior with increasing defect concentration was also observed in $Ti_{50}(Pd_{50-x}Mn_x)$ alloys, see Fig. 2. Below the Mn

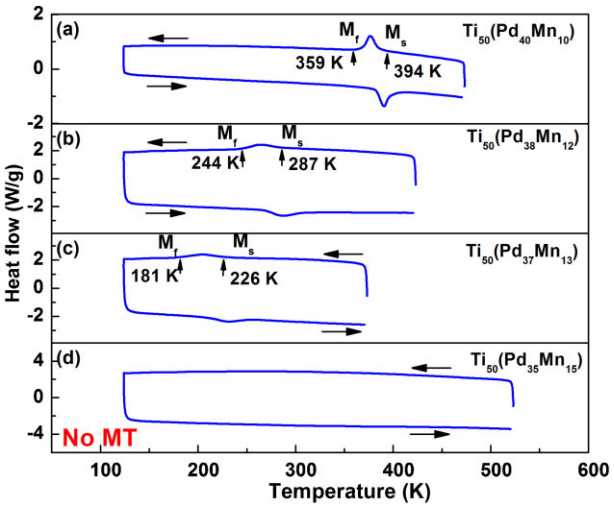

Figure 2 (a–d) DSC curves of $Ti_{50}(Pd_{50-x}Mn_x)$ ($x = 10$, 12, 13, 15) alloys, respectively. MT represents the martensitic transformation. M_s and M_f stand for the starting and finishing temperature of B2–B19 martensitic transformation, respectively.

concentration of ~13 at%, the B2–B19 martensitic transformation is shown to exist, as evidenced by the exothermal/endothermic peaks in DSC results of Fig. 2a–c. Above the Mn concentration of ~13 at%, the normal martensitic transformation disappears, as suggested by the absence of the exothermal/endothermic peaks in DSC results of Fig. 2d.

3.2 Evidence for strain glass in $Ti_{50}(Pd_{50-x}D_x)$ alloys The decreasing of martensitic transformation temperature and the weakening of the transformation signature by doping defects in the $Ti_{50}(Pd_{50-x}Fe_x)$ and $Ti_{50}(Pd_{50-x}Mn_x)$ systems shown in Figs. 1 and 2 are similar to those observed in the defect doped $Ti_{50-x}Ni_{50+x}$, $Ti_{50}(Ni_{50-x}D_x)$ (D = Fe, Cr, Mn, Co) and $Ti_{50}(Pd_{50-x}Cr_x)$ system [1, 12, 25]. This indicates that strain glass transition likely appears in the heavily doped $Ti_{50}(Pd_{50-x}D_x)$ alloys. It is known that one important signature of strain glass is its dynamic freezing process from a dynamically disordered state to a frozen disordered state [1, 2]. Such dynamic freezing can be identified by the frequency dispersion of the AC mechanical anomalies [1, 2]. The glass transition temperature $T_g(\omega)$ measured at a frequency ω obeys the Vogel–Fulcher relation $\omega = \omega_0 \exp[-E_a/k_B(T_g - T_0)]$, where E_a is the activation barrier and T_0 is the ideal glass transition temperature at 0 Hz. In the following, DMA measurement was performed to the $Ti_{50}(Pd_{50-x}Fe_x)$ and $Ti_{50}(Pd_{50-x}Mn_x)$ alloys to check the possible strain glass transition.

For the typical martensitic transformation behavior in slightly doped $Ti_{50}(Pd_{50-x}D_x)$ alloys which undergo normal B2–B19 transformation, the storage modulus displays a sharp dip and the internal friction shows a sharp peak at the martensitic transformation temperature. Both the dip and the peak have no frequency dispersion in its dip or peak temperature, which is the typical characteristic of normal martensitic transformation [2].

For those seemingly "non-transforming" alloys with higher defect concentration, it will be confirmed in the following that they actually undergo a strain glass transition. Figure 3 shows the strain glass features measured by DMA for the $Ti_{50}(Pd_{36}Fe_{14})$ alloy. The storage modulus shows a frequency-dependent dip at a critical temperature (glass transition temperature T_g) and the internal friction shows a frequency-dependent peak at temperature lower than T_g. The frequency dependence of $T_g(\omega)$ follows the Vogel–Fulcher relation, as shown in the inset of Fig. 3. The fitting yields an ideal freezing temperature T_0 of 227 K. The similar glassy feature can be also found in $Ti_{50}(Pd_{35}Mn_{15})$ alloy as shown in Fig. 4. The storage modulus and the internal friction all show clear frequency dispersion; and the fitting by Vogel–Fulcher relation yields an ideal freezing temperature T_0 of 233 K for $Ti_{50}(Pd_{35}Mn_{15})$ alloy, as shown in the in set of Fig. 4.

It should be noted that, T_g corresponding to the frequency range of 0.2–20 Hz for both $Ti_{50}(Pd_{36}Fe_{14})$ and $Ti_{50}(Pd_{35}Mn_{15})$ alloys are located at 265–300 K, which is within the ambient temperature range.

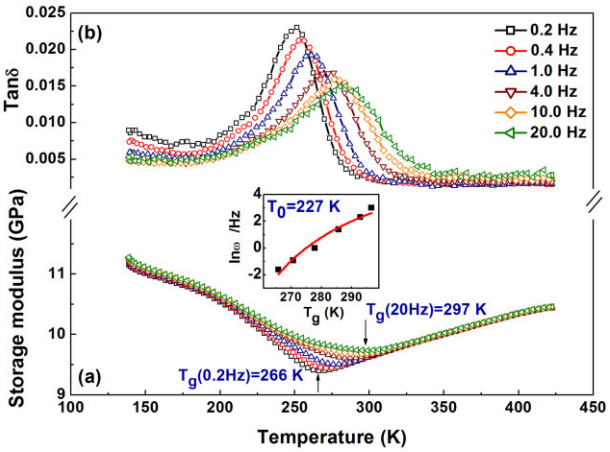

Figure 3 DMA results for $Ti_{50}(Pd_{36}Fe_{14})$ alloy. It shows the strong frequency dispersion of the storage modulus dip temperature T_g and internal friction peak temperature. Inset shows fitting of $T_g(\omega)$ using Vogel–Fulcher relation, where the ideal freezing temperature $T_0 = 227$ K.

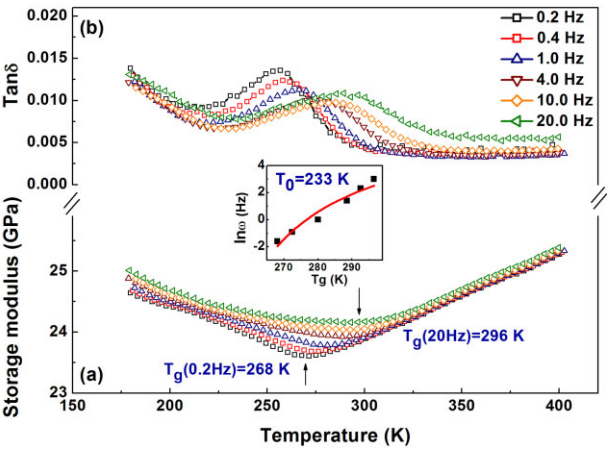

Figure 4 DMA results for $Ti_{50}(Pd_{35}Mn_{15})$ alloy. It shows the strong frequency dispersion of the storage modulus dip temperature T_g and internal friction peak temperature. Inset shows fitting of $T_g(\omega)$ using Vogel–Fulcher relation, where the ideal freezing temperature $T_0 = 233$ K.

3.3 Comparison of damping behaviors associated with normal martensitic transformation and strain glass transition Besides the shape memory effect and superelasticity, martensitic alloys are of considerable importance as promising high damping alloys, since they exhibit both high damping capacity and good mechanical properties [27–29]. There is a high damping peak associated with the martensitic transformation, which results from the hysteretic movement of twin boundaries and the interface between parent phase and martensite phase under AC external stress field [30, 31]. As shown in the above, there is also a damping peak associated with the strain glass

transition, which is due to the movement of twin boundaries between nanodomains and the interface between parent phase and nanodomains as well. Since the martensitic transition is a thermodynamic transition while the strain glass transition is a non-thermodynamic transition but a kinetics governed freezing process, it is interesting to compare their corresponding damping behavior during these two different transitions.

For some practical applications, their thermal hysteresis and cooling rate dependence are important aspects for evaluating the damping materials. Therefore, the damping behavior associated with these two kinds of transitions in these two aspects will be compared. The B2–B19 martensitic transition in $Ti_{50}(Pd_{45}Cr_5)$ alloy and the room temperature T_g strain glass transition in $Ti_{50}(Pd_{40}Cr_{10})$ alloy are selected as the typical examples.

In order to compare the intrinsic thermal hysteresis between cooling and heating, the internal friction is measured during step cooling and step heating, during which the sample is kept at every measuring temperature for 5 min to reach thermal equilibrium and then changed the frequency from 0.2 to 20 Hz discretely. Figure 5a shows the internal friction during B2–B19 martensitic transition. It can be seen that there is a large thermal hysteresis (~10 K) between the damping peak on cooling and heating processes, which is one of the main features of the first order martensitic transformation, because it involves a large transformation lattice strain. On the contrary, for the strain glass transition in Fig. 5b, the internal friction peak on cooling and heating reveals nearly zero thermal hysteresis, which can be ascribed to the very small and local lattice strains within the nanodomains. The near zero thermal hysteresis makes the strain glass to be superior to the normal martensitic alloys for potential damping applications.

In order to compare the cooling rate dependence of the damping properties, the internal friction was measured at a cooling rate of 2 K min^{-1} and step-cooing, respectively. The results are shown in Fig. 6a and b. Clearly, the damping

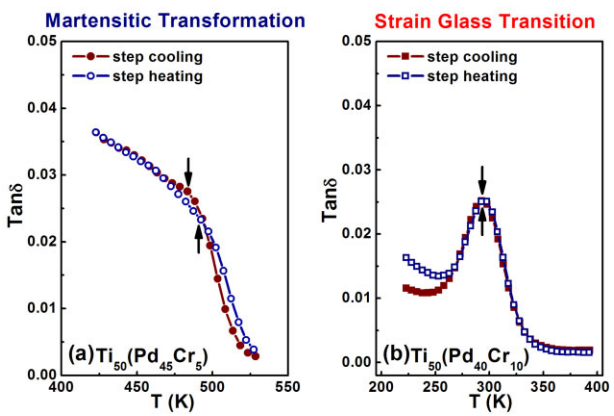

Figure 5 Comparison of thermal hysteresis of the damping behavior associated with the normal B2–B19 martensitic transformation in $Ti_{50}(Pd_{45}Cr_5)$ (a) and strain glass transition in $Ti_{50}(Pd_{40}Cr_{10})$ (b).The frequency used during measurement is 1 Hz.

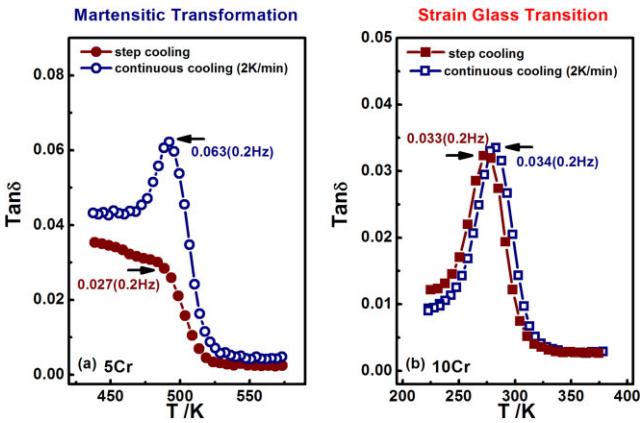

Figure 6 Comparison of cooling rate dependence of the damping behavior associated with the normal martensitic transformation (a) and strain glass transition (b).

capacity of martensitic transformation shows a strong cooling dependence, i.e. the damping value is half cut during step cooling in Fig. 6a, while that of strain glass transition shows almost fully cooling rate independence in Fig. 6b. Therefore, in order to keep a stable damping capacity for applications in an environment with variable cooling rate, strain glass is also superior to martensitic alloys.

In summary, the damping behaviors associated with the strain glass transition shows nearly zero thermal hysteresis and little cooling rate dependence. Such stable damping capacity suggests that strain glass alloys are promising damping materials. Furthermore, strain glass transition can occur at both ambient temperatures(TiPd-based alloys) and cryogenic temperatures (TiNi-based alloys); and they may find potential applications.

4 Discussion

4.1 Generality of high temperature strain glass transition in defect doped TiPd-based alloys Based on the DSC and DMA results, the phase diagrams of the $Ti_{50}(Pd_{50-x}Fe_x)$ and $Ti_{50}(Pd_{50-x}Mn_x)$ systems are plotted and shown in Fig. 7a and b. And the previously reported phase diagrams of the $Ti_{50}(Pd_{50-x}Cr_x)$ system is also shown in Fig. 7c [12]. It can be seen the evolution of phase transformation behaviors as a function of defect concentration in these three different systems shows a strikingly similar tendency. When defect concentration is lower than the critical value x_c, the system undergoes a B2–B19 martensitic transformation, but the corresponding transformation temperature M_s decreases drastically with increasing defect concentration. By contrast, when the defect concentration exceeds the critical value x_c, no B2–B19 martensitic transformation can be detected in these systems. Instead, they undergo a strain glass transition. The glass transition temperature T_0 also decreases with increasing defect concentration. It should be noted, although there exists a critical value x_c for each system, it is different for different kinds of dopant.

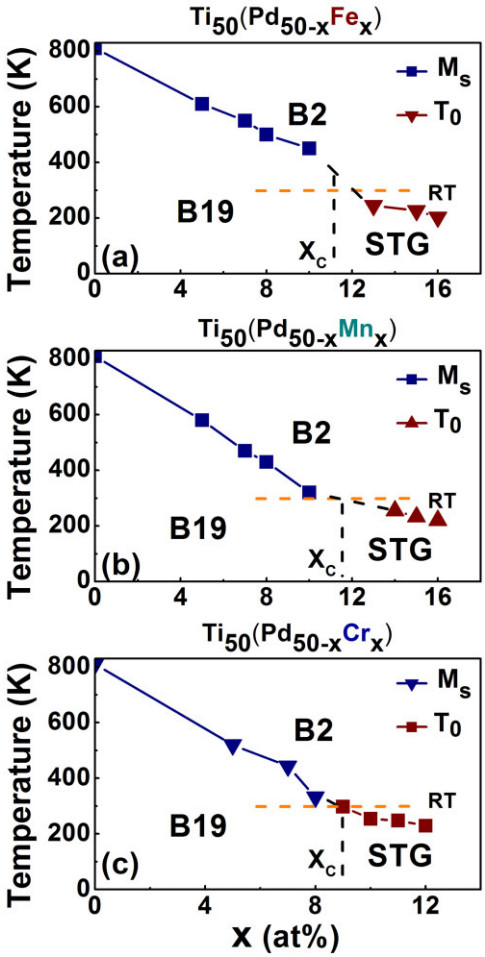

Figure 7 Temperature-composition phase diagrams of $Ti_{50}(Pd_{50-x}D_x)$ (D = Fe, Mn, Cr) alloys. When the defect concentration exceeds a critical value x_c for each system, the strain glass transition occurs. The ideal freezing temperature T_0 of these TiPd-based systems is around the ambient temperature. STG represents strain glass. The phase diagram of $Ti_{50}(Pd_{50-x}Cr_x)$ in (c) was previously proposed by Zhou et al. [12].

Such evolution of transformation behaviors as a function of defect concentration is similar with that of defect doped TiNi-based alloys, although the produced martensite phase is of different structure for TiNi-based and TiPd-based alloys [1, 12, 13]. The above systematic experimental confirmation of strain glass transitions in TiPd-based alloys further indicates that strain glass could be a general phenomenon in defect-doped martensitic systems. However, there exist an apparent difference between TiNi-based and TiPd-based strain glass alloys, that is, all TiPd-based strain glass alloys are characterized by a ambient-temperature T_0, which is decades higher than that of TiNi-based strain glass alloys [13].

The strain glass transition in these TiPd-based alloys can also be ascribed to the sufficient doping of point defects, which produce two necessary effects on strain glass formation, as discussed in our earlier work [13]. One is creating random local strain, because these defect atoms of different atomic size are randomly distributed in the crystal lattice. The existence of such random local strain hinder the formation of long range ordered martensite phase on cooling, but favors the strain glass formation with local ordering. The other one is reducing the thermodynamic stability of martensite phase. It can be seen that, doping of all these different kinds of point defects decreases the martensitic transformation temperature; this indicates that defect doping reduces the thermodynamic driving force for formation of martensite phase. As a result, with sufficient defect doping, the martensitic transformation is suppressed and strain glass transition occurs. Therefore, both effects impede the long range ordered martensite phase but favor the local ordered strain glass, which can also be understood by the phenomenological free energy landscape [12].

4.2 Possible factors influencing the strain glass transition temperature (T_0) Now the question arises: why TiPd-based strain glass alloys have a higher ideal freezing temperature T_0 than that of the TiNi-based strain glass alloys? In this subsection, we are going to list several possible factors, which may influence the strain glass transition temperature, including the M_s, elastic anisotropic factor and size of twinning shear of the host alloy.

Figure 8 shows the comparison of phase diagrams between these TiNi-based and TiPd-based alloys. As already shown in the above, the transformation behavior as a function of defect concentration x is very similar for these two kinds of systems. Below a critical defect concentration, increasing defect concentration only lowers the normal martensitic transformation temperature M_s; while above the critical defect concentration, the normal martensitic transformation vanishes and is replaced by a strain glass transition. However, there is a clear difference between the two systems. TiNi-based alloys start from the pure TiNi host alloy with a low M_s (~335 K), but TiPd-based alloys start from the pure TiPd host alloy with a much higher M_s (~810 K). Correspondingly, the former system ends up with a strain glass with low T_0 and the latter system ends up with a strain glass with much higher T_0. Therefore, T_0 of strain glass alloy seemingly has a close relationship with M_s of the host alloy without point defect doping.

Besides the M_s of the host alloys, Table 1 further compares the elastic anisotropy factor and size of twinning shear of the two host alloys. The elastic anisotropy factor (A), defined as the ratio between the two relevant shear moduli $A = C_{44}/C'$ [32], determines the long-range anisotropic interactions in the martensitic alloys [17]. The size of twinning shear (s), directly related with the mobility of twin boundary, somehow reflects the energy barrier between two twin variants [32]. From Table 1, it seems that larger elastic anisotropy factor and size of twinning shear (the case of TiPd-based alloys) of the host alloy correspond to the high glass transition temperature T_0; and smaller ones (the case of TiNi-based alloys) correspond to the low glass transition temperature T_0.

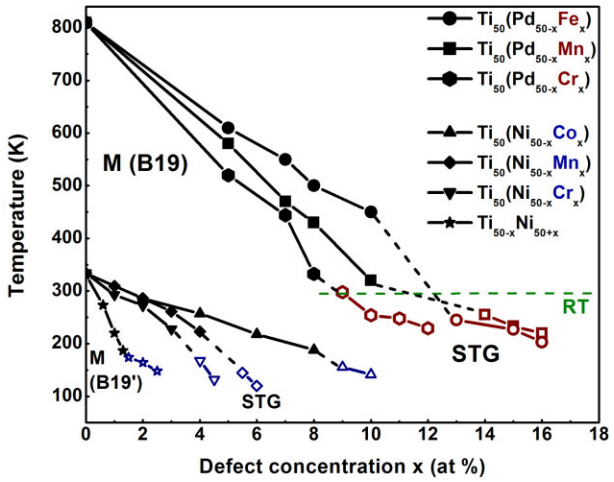

Figure 8 Comparison of transformation behaviors as a function of defect concentration between TiNi-based and TiPd-based alloys. The solid points stand for the starting temperature of martensitic transformation M_s and the empty point stand for the ideal freezing temperature T_0 of strain glass transition. M the represents martensite phase and STG represents strain glass. x is the defect concentration. RT represents the room temperature (~298 K).The data of $Ti_{50-x}Ni_{50+x}$, $Ti_{50}(Ni_{50-x}D_x)$, $Ti_{50}(Pd_{50-x}Cr_x)$ are from Refs. [1, 12, 13].

These facts may be preliminarily understood from the aspect of competition between the long-range anisotropic interaction (favors long-range ordered martensite) and the kinetic hindrance produced by doped point defects (favors short-range ordered STG). As shown in Fig. 8, for the Cr-doped TiPd-based alloy, the critical Cr concentration for the occurrence of strain glass is 9 at%, while that for the strain glass in Cr-doped TiNi-based alloys is only 3 at%. Such large difference may results from the contrasting M_s and elastic anisotropic factor of these two systems. High M_s indicates high martensite stability, i.e. large thermodynamic driving force for the formation of martensite phase; and the large elastic anisotropy factor corresponds to a strong long-range interaction. Therefore, larger amount of defect doping is required to suppress the formation of long range ordered martensite by destroying the strong long range interaction. Meanwhile, such larger amount of defect doping gives rise to the large energy barriers between nanodomains.

Table 1 Comparison of properties (martensitic transformation temperature, elastic anisotropy factor, and size of twinning shear) between TiNi and TiPd alloys.

	TiNi	TiPd
martensitic transformation temperature (M_s)	335 K	810 K
elastic anisotropy factor (A)	2.0[a]	3.6[b]
size of twinning shear (s)	0.280[a]	0.361[b]

[a]from Ref. [32].
[b]from Refs. [33, 34].

The delicate competition between the long-range interaction and the kinetic hindrance at certain thermal activation energy level will determine the glass transition temperature. However, how these factors and other possible factors determine the strain glass transition temperature in detail is far from recovered and further simulation studies may be helpful to clear such mystery.

Practically, the correspondence between M_s of the pure host alloy and T_0 of the corresponding strain glass alloy can be used to design strain glass alloys with proper T_0: high T_0 can be obtained by doping point defects into a host alloy with high M_s. Note that the cost of the present TiPd alloys is very high; thus applying the guideline in other low cost systems to achieve strain glass with proper T_0 will increase the applicability.

5 Conclusions In order to develop high T_0 strain glass alloys, systematic studies have been done on the phase transformation behaviors of defect (Fe, Mn, Cr) doped TiPd alloys, by means of DSC and DMA. The obtained results and conclusions are presented in the following.

(1) Despite different kinds of point defect, all systems show a similar tendency of transformation behaviors: below the critical defect concentration x_c, the martensitic transformation temperature decreases with increasing defect concentration; above x_c, the martensitic transformation is suppressed and they all undergo a strain glass transition, although the x_c is different for different kinds of defect doped systems.
(2) The existence of strain glass transition in these TiPd-based alloys further suggests that strain glass could be a general phenomenon in defect-doped ferroelastic systems.
(3) All TiPd-based strain glass alloys have a high freezing temperature within the ambient temperature range, which is much higher than that of TiNi-based strain glass alloys.
(4) T_0 of strain glass alloy is closely related with the martensitic transformation temperature M_s (i.e. martensitic stability) of its corresponding undoped host alloy. This may provide a guideline for designing strain glass with desired T_0 and achieving functionalities at desired temperatures.
(5) The damping behavior associated with strain glass transition shows near zero thermal hysteresis and little cooling rate dependence, which suggests that strain glass alloys are promising damping materials under variable environment.

Acknowledgements The authors gratefully acknowledge the support of National Basic Research Program of China (Grant No. 2012CB619401 and No. 2010CB631003), National Natural Science Foundation of China (Grant No. 51201126, No.51302209, No. 51321003, No. 51171140, and No. 51231008), and 111 project of China (B06025).

References

[1] S. Sarkar, X. Ren, and K. Otsuka, Phys. Rev. Lett. **95**, 205702 (2005).
[2] X. Ren, Y. Wang, Y. Zhou, Z. Zhang, D. Wang, G. Fan, K. Otsuka, T. Suzuki, Y. Ji, J. Zhang, Y. Tian, S. Hou, and X. Ding, Philos. Mag. **90**, 141 (2010).
[3] D. Wang, Y. Wang, Z. Zhang, and X. Ren, Phys. Rev. Lett. **105**, 205702 (2010).
[4] Z. Zhang, Y. Wang, D. Wang, Y. Zhou, K. Otsuka, and X. Ren, Phys. Rev. B **81**, 224102 (2010).
[5] R. Vasseur, D. Xue, Y. Zhou, W. Ettoumi, X. Ding, T. Lookman, and X. Ren, Phys. Rev. B **86**, 184103 (2012).
[6] D. Sherrington, Disorder and Strain-induced Complexity in Functional Materials (Springer, Berlin, Germany, 2012), p. 177.
[7] R. N. Bhowmik and R. Ranganathan, J. Magn. Magn. Mater. **248**, 101 (2002).
[8] R. Zhang, J. F. Li, and D. Viehland, J. Am. Ceram. Soc. **87**, 864 (2004).
[9] H. Uršič and D. Damjanovic, Appl. Phys. Lett. **103**, 072904 (2013).
[10] A. Saxena, Integr. Ferroelectrics **131**, 3 (2011).
[11] Y. Wang, X. Ren, K. Otsuka, and A. Saxena, Phys. Rev. B **76**, 132201 (2007).
[12] Y. Zhou, D. Xue, X. Ding, K. Otsuka, and X. Ren, Appl. Phys. Lett. **95**, 151906 (2009).
[13] Y. Zhou, D. Xue, X. Ding, Y. Wang, J. Zhang, Z. Zhang, D. Wang, K. Otsuka, and X. Ren, Acta Mater. **58**, 5433 (2010).
[14] Y. Wang, C. Huang, J. Gao, X. Ding, X. Song, and X. Ren, Appl. Phys. Lett. **101**, 101913 (2012).
[15] Y. Zhou, D. Xue, Y. Tian, X. Ding, S. Guo, K. Otsuka, J. Sun, and X. Ren, Phys. Rev. Lett. **112**, 025701 (2014).
[16] D. Schryvers, S. Cao, S. Pourbabak, H. Shi, and J. B. Lu, J. Alloys Compd. **577**, S705 (2013).
[17] P. Lloveras, T. Castán, P. Marcel, A. Planes, and A. Saxena, Phys. Rev. Lett. **100**, 165707 (2008).
[18] P. Lloveras, T. Castán, P. Marcel, A. Planes, and A. Saxena, Phys. Rev. B **80**, 054107 (2009).
[19] R. Vasseur and T. Lookman, Phys. Rev. B **81**, 094107 (2010).
[20] R. Vasseur, T. Lookman, and S. R. Shenoy, Phys. Rev. B **82**, 094118 (2010).
[21] D. Sherrington, arXiv:0801.2188 (2008).
[22] Y. Wang, X. Ren, and K. Otsuka, Phys. Rev. Lett. **97**, 225703 (2006).
[23] Y. Wang, X. Song, X. Ding, S. Yang, J. Zhang, X. Ren, and K. Otsuka, Appl. Phys. Lett. **99**, 051905 (2011).
[24] Y. Ji, X. Ding, T. Lookman, K. Otsuka, and X. Ren, Phys. Rev. B **87**, 104110 (2013).
[25] D. Wang, Z. Zhang, J. Zhang, Y. Zhou, Y. Wang, X. Ding, Y. Wang, and X. Ren, Acta Mater. **58**, 6206 (2010).
[26] K. Otsuka and C. M. Wayman, Shape Memory Materials (Cambridge University Press, Cambridge, 1998).
[27] G. Mazzolai, AIP Adv. **1**, 040701 (2011).
[28] Y. Zhou, G. Fan, D. Xue, X. Ding, K. Otsuka, J. Sun, and X. Ren, Scr. Mater. **61**, 805 (2009).
[29] G. Fan, Y. Zhou, K. Otsuka, and X. Ren, Appl. Phys. Lett. **89**, 161902 (2006).
[30] J. S. Juan, M. L. No, and C. A. Schuh, Nature Nanotechnol. **4**, 415 (2009).
[31] E. K. H. Salje, H. Zhang, H. Idrissi, D. Schryvers, M. Carpenter, X. Moya, and A. Planes, Phys. Rev. B **80**, 134114 (2009).
[32] K. Otsuka and X. Ren, Prog. Mater. Sci. **50**, 511 (2005).
[33] S. M. Shapiro, B. X. Yang, Y. Noda, L. E. Tanner, and D. Schryvers, Phys. Rev. B **44**, 9301 (1991).
[34] M. Nishida, T. Hara, Y. Morizono, A. Ikeya, H. Kijima, and A. Chiba, Acta Mater. **45**, 4847 (1997).